Solution structure of the Zβ domain of human DNA-dependent activator of IFN-regulatory factors and its binding modes to B- and Z-DNAs

Kyungmin Kim[a,b], Bulat I. Khayrutdinov[b,c], Chung-Kyung Lee[b], Hae-Kap Cheong[b], Sung Wook Kang[a], Hyejin Park[a], Sangho Lee[d], Yang-Gyun Kim[e], JunGoo Jee[f], Alexander Rich[g,1], Kyeong Kyu Kim[a,1], and Young Ho Jeon[b,h,1]

[a]Department of Molecular Cell Biology, Samsung Biomedical Research Institute, Sungkyunkwan University School of Medicine, Suwon 440-746, Korea; [b]Magnetic Resonance Team, Korea Basic Science Institute, Ochang, Chungbuk 363-883, Korea; [c]Department of General Physics, Kazan State University, Kazan 420008, Republic of Tatarstan, Russian Federation; Departments of [d]Biological Science and [e]Chemistry, Sungkyunkwan University, Suwon 440-746, Korea; [f]Center for Priority Areas, Tokyo Metropolitan University, Tokyo 192-0397, Japan; [g]Department of Biology, Massachusetts Institute of Technology, Cambridge, MA 02139; and [h]College of Pharmacy, Korea University, Jochiwon, Chungnam 339-700, Korea

Contributed by Alexander Rich, October 28, 2010 (sent for review July 9, 2010)

The DNA-dependent activator of IFN-regulatory factors (DAI), also known as DLM-1/ZBP1, initiates an innate immune response by binding to foreign DNAs in the cytosol. For full activation of the immune response, three DNA binding domains at the N terminus are required: two Z-DNA binding domains (ZBDs), Zα and Zβ, and an adjacent putative B-DNA binding domain. The crystal structure of the Zβ domain of human DAI ($hZ\beta_{DAI}$) in complex with Z-DNA revealed structural features distinct from other known Z-DNA binding proteins, and it was classified as a group II ZBD. To gain structural insights into the DNA binding mechanism of $hZ\beta_{DAI}$, the solution structure of the free $hZ\beta_{DAI}$ was solved, and its bindings to B- and Z-DNAs were analyzed by NMR spectroscopy. Compared to the Z-DNA–bound structure, the conformation of free $hZ\beta_{DAI}$ has notable alterations in the α3 recognition helix, the "wing," and Y145, which are critical in Z-DNA recognition. Unlike some other Zα domains, $hZ\beta_{DAI}$ appears to have conformational flexibility, and structural adaptation is required for Z-DNA binding. Chemical-shift perturbation experiments revealed that $hZ\beta_{DAI}$ also binds weakly to B-DNA via a different binding mode. The C-terminal domain of DAI is reported to undergo a conformational change on B-DNA binding; thus, it is possible that these changes are correlated. During the innate immune response, $hZ\beta_{DAI}$ is likely to play an active role in binding to DNAs in both B and Z conformations in the recognition of foreign DNAs.

DNA can activate immune responses in the innate immune system. Nonmethylated CpG sequences are recognized by toll-like receptor 9, and this results in inducing type-I interferon (IFN) (1). Double-stranded DNA, when placed in the cytosol of a cell by invading microbes or left by incomplete clearance of DNA damage, also can evoke immune responses (2–4). A recent study demonstrated that, in addition, the DNA-dependent activator of IFN-regulatory factors (DAI), formerly known as DLM-1 or ZBP1, also detects cytosolic DNAs and activates the innate immune response (5). DAI mediates activation of the innate immune system by facilitating DNA-mediated induction of type-I IFN and the expression of other related genes. DAI contains three DNA binding domains in the N terminus: two Z-DNA binding domains (ZBDs), Zα and Zβ, and an adjacent D3 region, a putative B-DNA binding domain. The D3 region plays pivotal roles in DNA binding, but all three domains are indispensable for the full activation of DAI (6). An intriguing question in innate immunity is how diverse foreign DNAs in the B- or Z-DNA conformations can be efficiently recognized by the DNA binding domains of DAI.

For the last decade there have been extensive structural and biochemical studies on ZBDs. The editing enzyme ADAR1 (double-stranded RNA adenosine deaminase) was the first Zα-containing protein to be identified. Zα domains were also found in the vaccinia virus E3L protein (7) and in PKZ (protein kinase containing Z-DNA binding domain). Crystal structures of the Zα domains of ADAR1, DAI, and Yaba-like pox disease virus complexed with Z-DNAs have been reported (8–10). Solution structures of the DNA-free Zα domain from human $Z\alpha_{ADAR1}$ ($hZ\alpha_{ADAR1}$) and from vaccinia virus $Z\alpha_{E3L}$ ($vvZ\alpha_{E3L}$) are also available (11, 12). A typical Zα domain consists of an $\alpha+\beta$ helix-turn-helix motif and a β sheet. Z-DNA binding is mediated by helix α3, called the recognition helix; the tyrosine residue in the recognition helix is the centerpiece in this process. The β-loop between strands β2 and β3 participates in Z-DNA binding in conjunction with the recognition helix and forms the "wing" structure. The wing contains conserved proline residues that make hydrophobic contacts with the phosphate backbone of Z-DNA.

Contrary to the wealth of structural information on Zα domains, few studies have reported the structures of Zβ domains, the second Z-DNA binding domains identified in ADAR1, DAI, and PKZ. To date, the crystal structure of Zβ domain from human $Z\beta_{ADAR1}$ is known (13), but it lacks the central tyrosine on the recognition helix and does not have Z-DNA binding activity. In contrast, the Zβ domain of human DAI ($hZ\beta_{DAI}$) is unusual because it has Z-DNA binding activity, despite the lack of some residues that are known to be essential for Z-DNA binding in Zα domains (7, 14). The recent crystal structure of $hZ\beta_{DAI}$/Z-DNA complex revealed a unique mode of Z-DNA recognition (15), and thus it is considered to be one of the group II ZBDs.

In order to gain further structural insights into the unusual Z-DNA binding mode of $hZ\beta_{DAI}$, and to elucidate its DNA binding mechanism, we determined the solution structure of the DNA-free $hZ\beta_{DAI}$ and analyzed its binding to B- and Z-DNAs using NMR spectroscopy. Here, we show that $hZ\beta_{DAI}$ in solution exhibits structural deviations from the crystal structure of the complex, suggesting that $hZ\beta_{DAI}$ undergoes conformational alterations upon DNA binding. In addition, residues involved in the weaker B-DNA binding are revealed by chemical-shift perturbation (CSP) experiments, and its binding mode to B-DNA is proposed. These results provide clues for understanding how $hZ\beta_{DAI}$ contributes to the recognition of foreign DNA in the innate immune response.

Author contributions: K.K., K.K.K., and Y.H.J. designed research; K.K., B.I.K., C.-K.L., H.-K.C., S.W.K., J.J., and H.P. performed research; K.K., B.I.K., A.R., K.K.K., and Y.H.J. analyzed data; and K.K., S.L., Y.-G.K., A.R., K.K.K., and Y.H.J. wrote the paper.

The authors declare no conflict of interest.

Data deposition: The atomic coordinates and NMR constraints have been deposited in the Protein Data Bank, www.pdb.org (PDB ID code 2L4M).

[1]To whom correspondence may be addressed. E-mail: cbeckman@mit.edu, kkim@med.skku.ac.kr, or yhjeon@korea.ac.kr.

This article contains supporting information online at www.pnas.org/lookup/suppl/doi:10.1073/pnas.1014898107/-/DCSupplemental.

Results

Overall Structure of hZβ_{DAI} and Comparison to Other Z-DNA Binding Domains. We determined the three-dimensional solution structure of hZβ_{DAI} using NMR spectroscopy. The backbone RMSD of 20 lowest energy structures superimposed is 0.13 ± 0.04 Å (Table S1 and Fig. S1). The overall fold of hZβ_{DAI} in solutions appears similar to other known ZBDs with the canonical $\alpha + \beta$ helix-turn-helix motif consisting of three helices and three β-strands (called "winged helices") (Fig. 1*A*). The overall conformation of the DNA-free hZβ_{DAI} is similar with those of hZα_{ADAR1} and vvZα_{E3L} (Fig. 1*B*). Notable conformational differences are found in the recognition helix (α3) and the wing (β2 and β3), as previously observed for the crystal structure of hZβ_{DAI} complexed with Z-DNA, in comparison with other ZBD/DNA complexes (15). It appears that the recognition helix of hZβ_{DAI} is bent with a mixed conformation of 3_{10}- and α-helices, rather than a straight α-helix, and the tip of the wing is seen to pull out of the canonical position critical in Z-DNA binding (Fig. 1*B*). The residual dipolar coupling (RDC) experiments also confirmed that the DNA-free hZβ_{DAI} has a bent helix rather than a straight helix (Table S2 and Fig. S2). In this analysis, the RDC values calculated from a modified structure containing the recognition helix in a straight conformation showed larger deviations than those calculated from the NMR or X-ray structures (Fig. S2).

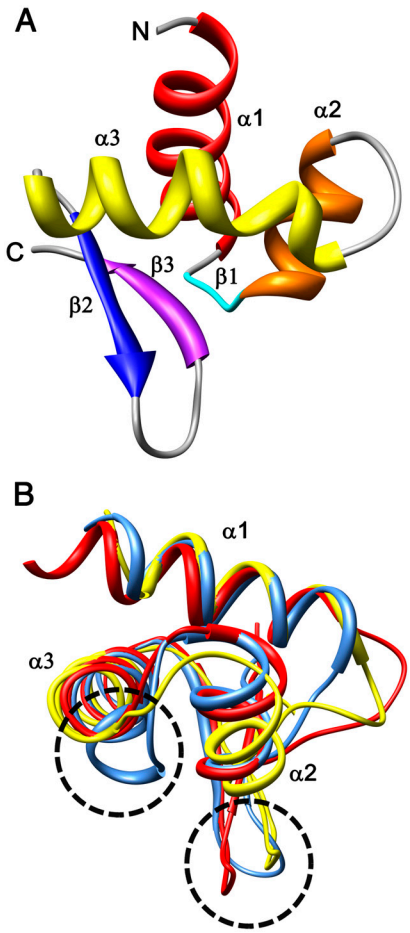

Fig. 1. The solution structure of free hZβ_{DAI} and structural comparison with homologous proteins. (*A*) The solution structure of free hZβ_{DAI} is represented in the ribbon diagram. It contains an $\alpha + \beta$ helix-turn-helix fold typical of B-DNA binding proteins. (*B*) Superimposition of the solution structures defined by NMR spectroscopy, free hZβ_{DAI}, free hZα_{ADAR1}, and free vvZα_{E3L} (blue, red, and yellow, respectively). Dashed black circles indicate the N-terminal region of α3 and β turns.

Conformational Changes of hZβ_{DAI} upon Z-DNA Binding. From the crystal and solution structures of hZα_{ADAR1}, it is known that Zα does not show any significant conformational changes upon Z-DNA binding, which indicates that it is a prepositioned binding surface for Z-DNA (11). However, hZβ_{DAI} shows notable changes in the N-terminal region of the recognition helix (Fig. 2*A* and Fig. S3). This suggests that conformational rearrangements occur in the DNA-recognition regions upon DNA binding. Free and DNA-bound hZβ_{DAI} commonly have a 3_{10}-helix (T136–D139) at the N-terminal end of the α3-helix; however, they display distinct conformations. Whereas the helicity of the recognition helix is well maintained in the free hZβ_{DAI} via hydrogen bonds between the N-terminal 3_{10}-helix and the C-terminal α-helix, the helicity is broken in the DNA-bound hZβ_{DAI} because of the absence of such backbone hydrogen bonds (Fig. S3*A*) (15). In the free hZβ_{DAI}, the backbone carbonyl oxygens of A137 and K138 in the 3_{10}-helix form hydrogen bonds with the side chain and backbone NH groups of N141 in the α3-helix of 2.9 and 3.6 Å, respectively. But, in the case of the DNA-bound hZβ_{DAI}, the distance between the backbone carbonyl oxygen of K138 and the backbone NH group of N141 is 4.1 Å, and the side chain NH group of N141 no longer forms a hydrogen bond with A137 because of the interaction with DNA [Protein Data Bank (PDB)

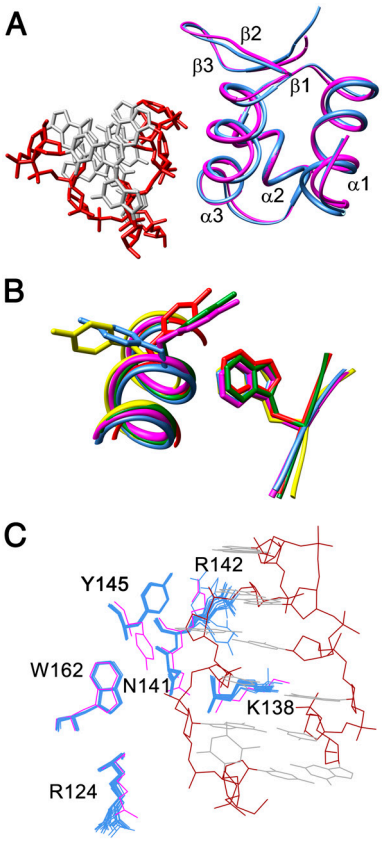

Fig. 2. Comparison of the free and DNA-bound hZβ_{DAI} structures. (*A*) Superimposition of the free (blue) and DNA-bound (magenta) hZβ_{DAI} structures (15). Z-DNA is depicted by a stick diagram. The secondary structures are labeled. (*B*) Comparison of the tyrosine conformation on the α3-helix in Z-DNA binding proteins; free hZβ_{DAI} and hZα_{ADAR1} (blue and red, respectively) and DNA-bound hZβ_{DAI} and hZα_{ADAR1} (magenta and green, respectively), and free vvZα_{E3L} (yellow). The tyrosine residue in Z-DNA bound structures (magenta and green) shows CH-π interactions (17) with the tryptophan residue in the β3-strand. A similar conformation is found with the free hZα_{ADAR1} structure (red). (*C*) Superimposition of six residues contacting Z-DNA in the hZβ_{DAI}/Z-DNA complex (magenta) (15) with those in the ensemble of 20 lowest energy structure of free hZβ_{DAI} (blue). The Z-DNA backbone is in dark red; bases are in gray.

ID code 3EYI, chain A]. The conformational change of the 3_{10}-helix in the DNA-bound hZβ_{DAI} was also confirmed by measuring the distances between Cα atoms in the 3_{10}-helix and the α3-helix (Table S3). The solution conformation would not be favorable for Z-DNA interaction because K138 and R142, which play a pivotal role in Z-DNA binding, point away from the DNA backbone (Fig. S3*B*). However, Z-DNA binding causes the extension of the N-terminal 3_{10}-helix and the proper binding of K138 and R142 to Z-DNA (Fig. S3*A*). It is thought that these conformational changes could be occurring because the energy gained by the interactions of K138, N141, and R142 with the phosphate backbone of Z-DNA is more than the energy loss caused by the dissociation of the hydrogen bond between the side chain of N141 and the carbonyl group of A137 and the backbone hydrogen bond in K138/N141.

The tyrosine residue in the recognition helix is also critical in Z-DNA binding (8–12, 16). The conserved tyrosine confers CH-π interactions with both the edge of the tryptophan residue (17) in the β3-strand and the guanosine base in the *syn*-conformation in Z-DNA. Although the conserved tyrosine was observed to be in contact with Z-DNA in the Z-DNA complex structure of yatapox virus Zα_{E3L} (10), it was proposed that the conformation of the vaccinia tyrosine residue in the free state vvZα_{E3L} is strongly correlated with the lack of Z-DNA converting activity (12). Whereas hZα_{ADAR1} has a prepositioned tyrosine to interact with Z-DNA even in the free state and shows high Z-DNA converting activity (11), vvZα_{E3L} has the solvent-exposed tyrosine conformation with diverse rotamers, and its Z-DNA converting activity is reduced (12) (Fig. 2*B*). In the free hZβ_{DAI}, the corresponding Y145 does not overlap with that of the DNA-bound hZβ_{DAI}, but adopts a conformation close to that of vvZα_{E3L} (Fig. 2*B*). Therefore, it is suggested that the nonprepositioned conformation of Y145 in the free hZβ_{DAI} may be one of the reasons for the lower Z-DNA converting activity of hZβ_{DAI} than that of hZα_{ADAR1}. Consistently, hZβ_{DAI} appears to have lower binding affinity to Z-DNA and slower kinetics in Z-DNA converting activity (18, 19) than hZα_{ADAR1}.

Overall, hZβ_{DAI} seems to have a more flexible binding surface than hZα_{ADAR1}. Among the nine residues of hZα_{ADAR1} that are directly involved in DNA contact in the crystal structure of the complex, seven are already prepositioned in a free state (11). However, in the case of hZβ_{DAI}, four out of six Z-DNA contacting residues (R124, K138, R142, and Y145) rearrange upon Z-DNA binding, and only N141 and W162 are prepositioned (Fig. 2*C*).

Conformational Isomerization of the DNA-Free hZβ_{DAI}. The ^{1}H-^{15}N heteronuclear single quantum coherence (HSQC) spectrum analysis of the free hZβ_{DAI} showed that there are more than two sets of NMR signals, which indicates the existence of conformational isomers (Fig. S4*A*). It was found by analysis of the nuclear Overhauser enhancement spectroscopy (NOESY) spectra that this phenomenon is due to the *cis-trans* isomerization of proline residues. Analysis of chemical-shift differences between the major and minor signals along the residues revealed that the differences are larger near the proline residue, P122 (Fig. S4*B*). The large chemical-shift difference between major and minor signals from I164 could also be explained by the fact that I164 is close to P122 in three-dimensional space. To verify the presence of proline isomerization and test the functional role of this residue, the P122 residue was mutated to alanine and its NMR spectrum and Z-DNA converting activity were examined. Interestingly, the minor signals from the wild-type hZβ_{DAI} were not seen in the ^{1}H-^{15}N HSQC spectrum of the P122A mutant (Fig. S4*A*), thereby confirming that those signals were caused by the *cis-trans* isomerization of P122. However, P122A mutant did not show any functional difference in terms of Z-DNA conversion activity measured by CD spectroscopy, compared to the wild-type protein (Fig. S4*C*). Those findings suggest that the proline isomerization is not relevant to the Z-DNA converting activity of hZβ_{DAI}. Consistently, both *cis*- and *trans*-isomers were observed in the crystal structure of the hZβ_{DAI}/Z-DNA complex (15). Therefore, it is thought that both isomers are in equilibrium in solution and both contribute to Z-DNA binding. RDC data also support the presence of the two isomers in solution; that is, the experimental RDC value for E121 (4.0 Hz) is the middle of the calculated RDC values of the *trans*-conformer (−0.7 Hz) and the *cis*-conformer (8.1 Hz). The mechanism underlying the enhancement of Z-DNA conversion activity by proline isomerization and its functional role remains to be studied.

CSPs upon B- and Z-DNA Binding. An intriguing question to ask is how the ZBD converts B-DNA to Z-DNA. As for the role of the ZBD in Z-DNA conversion, there have been different explanations. The ZBD might take an active part in Z-DNA conversion by binding to B-DNA first and initiating the conversion process. Alternatively, the ZBD could be more passively involved; that is, it may bind to the preformed Z-DNA that might be transiently formed by Brownian motion and shift the B–Z equilibrium toward Z-DNA. In either case, the positively charged surface of the ZBD is expected to be involved in DNA binding. Regarding the role of DAI in the recognition of foreign DNA, it was anticipated that the ZBD would bind to various conformations of DNA (5). To obtain structural insight into the B-DNA binding mode of hZβ_{DAI} and possibly into the B-to-Z converting mechanism, CSP experiments with hZβ_{DAI} were performed in the presence of double-stranded $(dCdG)_6$ (referred to as CG6), a Z-DNA forming sequence, and double-stranded $(dCdCdG)(dAdT)_6(dCdGdG)$ (referred to as AT6), a B-DNA forming one (Fig. 3 and Fig. S5). One-dimensional imino proton NMR and CD spectroscopy confirmed that CG6 formed Z-DNA upon the addition of hZβ_{DAI} (Fig. S5*A*) in the same way as observed for hZα_{ADAR1} (20). Whereas resonances of the imino protons of CG6 changed during the titration of hZβ_{DAI}, AT6 showed no changes except the intensity reduction by the line broadening effect of hZβ_{DAI} binding. The B-to-Z transition of CG6 induced by hZβ_{DAI} binding was also monitored by CD spectra. The molar ellipticity exhibited significant alterations at 255 and 295 nm, which is characteristic of Z-DNA. However, no spectral change was observed in the case of AT6.

The CSPs for backbone amide signals in ^{1}H-^{15}N HSQC and the aliphatic side chain signals in ^{1}H-^{13}C HSQC were quantified and displayed on the ribbon models and surface diagrams of the free hZβ_{DAI}, respectively (Fig. 3 *A* and *B*). When the protein is bound to CG6 as a Z-DNA, the backbone amides of the residues from T136 to R146 in the α3 helix showed significant perturbations. These results can be anticipated from the fact they are located in the N-terminal region of the α3 recognition helix and have critical roles in Z-DNA binding (Fig. 3*A*). Surprisingly, A137–D143 were also strongly perturbed by AT6 as a B-DNA, which suggests that they may be involved in binding to B-DNA as well as to Z-DNA. Whereas the residues located in the N-terminal region of the α3 helix are important in the binding both CG6 and AT6, the backbone amide groups in the middle part of α3 helix (Y145, R146, and M147) and two β-strands (D154, D156, K160, W162, T163, and Y165) region seem to have preference to CG6 because they showed large CSP values only upon CG6 binding. In addition, residues 107–112 and 107–110 of α1 helix showed perturbation in CG6 and AT6 binding, respectively. Together with residue 126 of the α2 helix, the residues in the N-terminal part of the α1 helix interact with both Z- and B-DNA nonspecifically. Overall, Z-DNA binding showed CSP in a larger area than on B-DNA binding including the β-sheet, whereas B-DNA binding occurs mainly in the region near to the N-terminal of α3 helix.

The crystal structure of the hZβ_{DAI}/Z-DNA complex reveals a noncanonical DNA binding mode in that the wing is pulled away

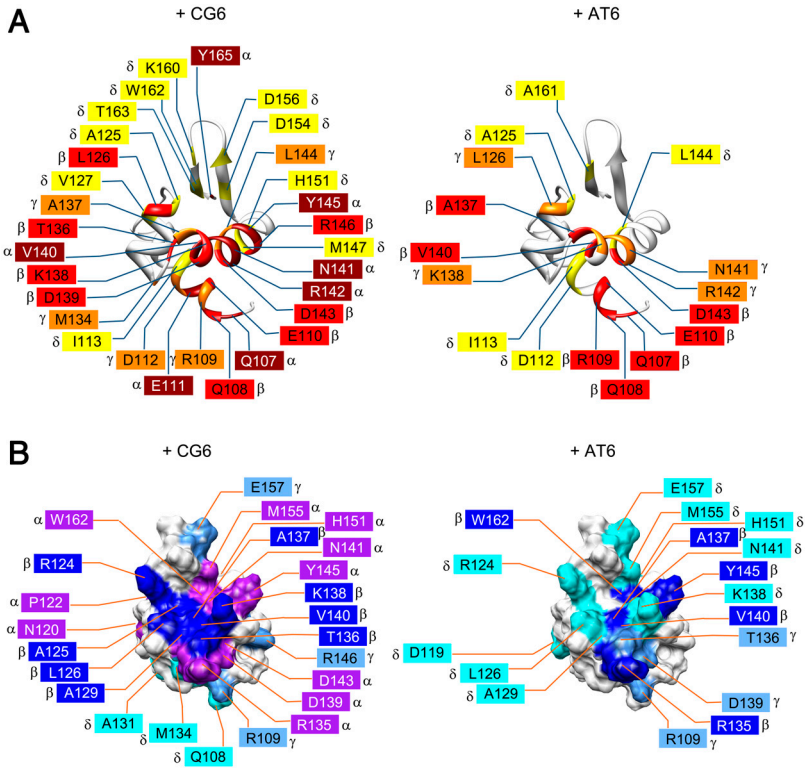

Fig. 3. DNA binding experiments with CG6 and AT6. (*A*) Ribbon diagrams indicating the residues that show chemical-shift perturbations ($\Delta\delta$) of the backbone; hZβ_{DAI} with CG6 (*Left*) and hZβ_{DAI} with AT6 (*Right*) (α, dark red, disappeared; β, red, ≥0.14 ppm; γ, orange, ≥0.10 ppm; δ, yellow, ≥0.06 ppm). (*B*) Surface mapping of the residues that show chemical-shift perturbations of the aliphatic side chains; hZβ_{DAI} with CG6 (*Left*) and hZβ_{DAI} with AT6 (*Right*) (α, purple, disappeared; β, blue, ≥0.10 ppm; γ, light blue, ≥0.075 ppm; δ, cyan, ≥0.05 ppm).

from the DNA (15). However, the hZβ_{DAI} mutant (E157A/ΔQ158/ΔS159/K160A) showed dramatic decreases in both Z-DNA binding and conversion activity (19). This observation prompted us to hypothesize that the wing structure may be involved in Z-DNA recognition to some extent via a mechanism yet unknown. CSP experiments upon addition of CG6 revealed significant changes in signals of both backbone atoms for the wing residues, H151, D154, D156, K160, W162, and T163, and side chain atoms from H151, M155, D156, E157, and W162, although they are not in direct contact with Z-DNA in the complex structure (15) (Fig. 3 *A* and *B* and Fig. S6). These findings may be explained by the fact that DNA binding could affect the magnetic environment of the wing directly or indirectly. H151, which is located near the hinge between α3 and the wing, showed altered conformations in the free and the DNA-bound hZβ_{DAI}. Thus, DNA-induced conformational changes in the wing might affect the conformation of H151. The CSP of the side chain of M155 seems to be due to the CH-π or hydrophobic interaction of M155 with W162, a key residue in Z-DNA binding. Additionally, on CG6 binding, R146 and D143 show large CSPs on both backbone and side chain signals, which is consistent with the fact that these two residues form a salt bridge upon Z-DNA binding (15). In the free hZβ_{DAI}, they are not salt-bridged but exposed to the solvent, as shown by their chemical-shift values, which are in the average range. Intriguingly, although the backbone signals were not perturbed significantly, the side chains of Y145 and W162 showed strong perturbation by the B-DNA binding as well as Z-DNA binding, which implies that these side chains are closely involved in the DNA contact before B–Z transition. This situation may facilitate the conformational change of Y145 in B–Z transition, resulting in the aromatic ring of Y145 positioned to have the CH-π interactions with both the edge of the W162 and guanosine base of Z-DNA.

Discussion

This study clearly demonstrated that hZβ_{DAI} undergoes conformational adaptations such as the movement of the wing and the recognition helix upon Z-DNA binding. Such changes were not expected because it was believed that ZBDs have a prefixed DNA binding interface, as found for hZα_{ADAR1} (11). In addition, Y145 is not prepositioned in hZβ_{DAI}. In the free state, Y145 of hZβ_{DAI} interacts with the side chain of neighboring R146. Cζ of Y145 is located near Cγ of R146 with a distance of 3.7 Å. Upon Z-DNA binding, the aromatic ring of Y145 moves to become sandwiched between the guanidine base of Z-DNA and the aromatic ring of W162, forming two stabilizing CH-π interactions (17). This movement affects the side chains of W162 and M155, and, in turn, the backbone of the wing from D154 to T163. In addition, the side chain of H151 in the hinge region was affected because of the movement of the wing region, resulting in large CSPs of the NMR signals. A somewhat related conformational change might take place when vvZα_{E3L} binds to Z-DNA, as its analogous tyrosine is flipped away from its binding position in the free state (12) (Fig. 2*B*).

Residues of hZβ_{DAI} involved in B-DNA binding were identified, and the mode of B-DNA binding was partially revealed. Based on the CSP experiment with B-DNA, its B-DNA binding mode may be related to the initial stage of the binding to Z-DNA forming sequences in the B-conformation. The charged residues in the N terminus of the α3 recognition helix may thus be important for the initial recognition of both B- and Z-conformations of DNA. However, there were subtle differences in the CSPs of B- and Z-DNA binding, which may be attributable to structural differences in the two DNA forms. These results support the idea that hZβ_{DAI} may have a unique B-DNA binding mode, distinct from the binding to Z-DNA. The wing, which is essential for Z-DNA binding, does not seem to be involved in binding B-DNA. Lack of additional interacting regions other than the recognition

helix might explain the relatively low binding affinity and relative nonspecificity of hZβ_{DAI} toward B-DNA. Indeed, the measurements of binding affinities by isothemal titration calorimetry revealed significantly higher binding affinity for Z-DNA, with K_d values of 226 nM and 16 μM to CG6 and AT6, respectively (Fig. S7 *A* and *B*). This result is consistent with the binding affinities estimated by CSPs. Binding to Z-DNA shows a slow to medium exchange binding pattern, whereas binding to B-DNA shows a fast exchange pattern (Fig. S5 *B* and *C*). Considering the interacting residues involved in B-DNA binding, which were identified from CSP experiments, hZβ_{DAI} could bind to the minor groove in a nonspecific manner (Fig. S7*C*), whereas virtually all B-DNA binding proteins bind to major grooves of B-DNA. In this binding model, the residues with a large CSP are located close to the phosphate backbone of B-DNA, which means that hZβ_{DAI} can have access to DNAs in the B-conformation without interacting with anything in the major groove. In the binding model to the major groove (Fig. S7*D*), K160 and Y145 collide with B-DNA, but R135 does not make any contact with it.

In the conversion mechanism to Z-DNA, when hZβ_{DAI} binds to CG6 in the B-DNA conformation, it may play an active role in initiating its conversion to the Z-DNA conformation. This is supported by the recent biophysical study of hZα_{ADAR1} (20). In that study, it was observed that the amounts of Zα-bound B-DNA and Zα-bound Z-DNA are the same and in equilibrium when the protein is limited. Then, the Z conformation of DNA is stabilized by additional binding of Zα to Z-DNA (20). A crystal structure of the B-DNA:Z-DNA junction revealed that at the junction one base pair was broken, and the two bases were extruded on either side of the DNA duplex (16). This base extrusion is likely to be central to initiating Z-DNA formation. Could that process be facilitated by B-DNA binding to ZBDs through its minor groove? Clearly, this is an avenue for further research.

Considering the function of DAI in the recognition of foreign DNA to boost the innate immune response (5), the conformational diversity and flexibility of hZβ_{DAI} may be an integral feature in recognizing foreign DNAs in various conformations. Because the domain on the C-terminal side of hZβ_{DAI} also undergoes a conformational change on binding DNA (5), these changes may be correlated. The current study contributes to understating the role of DAI at the molecular level in the innate immune system.

Materials and Methods

Protein Preparation. The Zβ domain (103–166) of human DAI (hZβ_{DAI}) and the double-stranded DNAs were prepared as described previously (15). Five extra amino residues (98-Ser-His-Met-Ala-Ser-102) were inserted during cloning. To produce isotopic labeled hZβ_{DAI}, bacteria were grown in M9 medium containing 1 g L^{-1} of $^{15}NH_4Cl$ and 2 g L^{-1} of ^{13}C-glucose (Cambridge Isotope Laboratories). After purification using Ni-NTA and HiTrap SP columns (GE Healthcare), double-labeled hZβ_{DAI} was dialyzed and concentrated in the NMR buffer [10 mM 2-(N-morpholino) ethanesulfonic acid (MES) pH 5.5, 10 mM NaCl]. The ^{15}N-labeled hZβ_{DAI} P122A mutant was also prepared in the same manner as the wild-type hZβ_{DAI}.

NMR Spectroscopy. NMR experiments were carried out at 35 °C on a 2 mM ^{13}C, ^{15}N-labeled protein sample in the NMR buffer containing 10% D_2O on Avance 900 MHz (Bruker). ^{1}H, ^{15}N, and ^{13}C-resonance assignments were obtained from the following three-dimensional heteronuclear correlation experiments: CBCA(CO)NH, HNCACB, HN(CA)CO, HNCO, HN(CO)CA, HNCA, HBHA(CO)NH, H(CCO)NH, C(CCO)NH, HCCH–correlation spectroscopy, and HCCH–total correlation spectroscopy (TOCSY). Distance restraints were derived from ^{15}N- or ^{13}C-resolved 3D NOESY. Aromatic side chains were assigned with aromatic ^{1}H-^{13}C HSQC and 2D ^{1}H-^{1}H TOCSY. Aromatic 3D ^{13}C-NOESY was used to produce the distance restraint. The dipolar coupling constants were obtained by taking the difference in the corresponding *J*-couplings measured in aligned hexanol-polyethylene glycol system wt = 4%, $r = 0.85$ and with splitting of D_2O 20.8 Hz (21, 22) and isotropic (water) media. $^1D_{NH}$-dipolar coupling constants were measured by recording 2D in-phase/antiphase ^{1}H-^{15}N transverse relaxation optimized spectroscopy spectra and $^1D_{CaCO}$ in IPAP-*J*-HNCO-based three-dimensional experiment (23, 24). NMR spectra were processed with NMRPipe (25) and analyzed with SPARKY 3.110 (26). For 1D imino proton NMR, samples were prepared by adding hZβ_{DAI} to 0.15 mM CG6 or AT6 dissolved in 10 mM MES pH 5.5, 50 mM NaCl to the indicated molar ratios of protein to DNA (P/N). The NMR spectra was taken at 500 MHz NMR (Bruker), and processed by SpinWorks 3.1.7 (27).

Structure Determination. Distance restraints were mainly derived from 3D ^{15}N- or ^{13}C-edited and 2D ^{1}H-^{1}H NOESY experiments. NOE assignment algorithm of CYANA 2.1 (28) performed both the structure calculation and the assignment of NOE peaks automatically. A total of 1,897 NOE-based upper distance restraints were gained. TALOS program (29) derived 110 backbone torsion angle restraints from chemical shifts. We obtained hydrogen bond restraints by H–D exchange experiment, and with these restraints, a total of 100 structures without significant violations were generated by CYANA 2.1. The structures were further refined by AMBER 10 (30) using an all-atom force field (ff99SB). The AMBER refinement consisted of three stages: 1,500 steps of energy minimization, 20-ps molecular dynamics, and 1,500 steps of energy minimization. The best 20 structures were selected as a final ensemble. A structure closest to the lowest energy was employed as representative. Final structures were well refined with a backbone and heavy atom RMSD of 0.13 and 0.69 Å, respectively, for residues 98–166. The structures also have good geometry with 92.3% of residues in the most favored region of the Ramachandran plot (Table S1) examined by PROCHECK (31). The N-terminal 10 residues were not well converged in the ensemble because of absence of long-range NOE.

Isothermal Titration Calorimetry. The CG6 and AT6 were dialyzed in 10 mM MES pH 5.5, 50 mM NaCl prior to the isothermal titration calorimetry experiments. The dissociation constant (K_d) for CG6 or AT6 was measured using a VP-ITC (MicroCal) at 25 °C.

CD Spectroscopy. The conversion of B- to Z-DNA was monitored by CD spectroscopy as described in the previous work (15) with slight modifications in 10 mM MES pH5.5, 50 mM NaCl. The B-to-Z conversion kinetics of the wild-type and P122A mutant were monitored using CG6 for 50 min at 255 nm at 25 °C in 10 mM MES pH 5.5, 150 mM NaCl.

CSP Experiment. We titrated 0.6 mM ^{15}N-labeled hZβ_{DAI} with CG6 and AT6 in a concentration of 0.035 mM, 0.075 mM, and 0.15 mM, respectively. ^{1}H-^{15}N HSQC spectra were collected for the backbone CSPs and ^{1}H-^{13}C constant time version HSQC spectra for aliphatic side chain CSPs. Both of them were performed in 10 mM MES pH 5.5, 50 mM NaCl at 35 °C. NMR resonances of ^{15}N, ^{13}C hZβ_{DAI} were affected along with increasing CG6 and AT6, respectively, in the following ways: (*i*) none or minimal change in chemical shift, (*ii*) vanished signal through medium exchange binding pattern, and (*iii*) major perturbation of chemical shift. Chemical-shift differences were calculated using the following equations: $\Delta\delta = \sqrt{(\Delta H)^2 + (0.2 \times \Delta N)^2}$ for backbone amide signals, and $\Delta\delta = \sqrt{(\Delta H)^2 + (0.5 \times \Delta C)^2}$ for aliphatic side chain signals.

ACKNOWLEDGEMENTS This work was supported by National Research Laboratory Program (NRL-2006-02287), Korea Research Foundation Grant (KRF-2008-220-C00040), 21C Frontier Functional Proteomics Program (FPR08B2-270), Korea Healthcare Technology Research and Development Project (A092006), and Ubiquitome Research Program (M105 33010001-05N3301-00100) to K.K.K. and Bio-MR research program and Global Frontier Project Grant NRF-M1AXA002-2010-0029765 to Y.H.J.

1. Takeda K, Kaisho T, Akira S (2003) Toll-like receptors. *Annu Rev Immunol* 21:335–376.
2. Ishii KJ, et al. (2006) A toll-like receptor-independent antiviral response induced by double-stranded B-form DNA. *Nat Immunol* 7:40–48.
3. Stetson DB, Medzhitov R (2006) Recognition of cytosolic DNA activates an IRF3-dependent innate immune response. *Immunity* 24:93–103.
4. Yoshida H, Okabe Y, Kawane K, Fukuyama H, Nagata S (2005) Lethal anemia caused by interferon-β produced in mouse embryos carrying undigested DNA. *Nat Immunol* 6:49–56.
5. Takaoka A, et al. (2007) DAI (DLM-1/DAI) is a cytosolic DNA sensor and an activator of innate immune response. *Nature* 448:501–506.
6. Wang Z, et al. (2008) Regulation of innate immune responses by DAI (DLM-1/ZBP1) and other DNA-sensing molecules. *Proc Natl Acad Sci USA* 105:5477–5482.
7. Kim YG, et al. (2003) A role for Z-DNA binding in vaccine virus pathogenesis. *Proc Natl Acad Sci USA* 100:6974–6979.
8. Schwartz T, Rould M, Lowenhaupt K, Herbert A, Rich A (1999) Crystal structure of the Zalpha domain of the human editing enzyme ADAR1 bound to left-handed Z-DNA. *Science* 284:1841–1845.

9. Schwartz T, Behlke J, Lowenhaupt K, Heinemann U, Rich A (2001) Structure of the DLM-1-Z-DNA complex reveals a conserved family of Z-DNA-binding proteins. *Nat Struct Biol* 8:761–765.
10. Ha SC, et al. (2004) A poxvirus protein forms a complex with left-handed Z-DNA: Crystal structure of a Yatapoxvirus Zalpha bound to DNA. *Proc Natl Acad Sci USA* 101:14367–14372.
11. Schade M, et al. (1999) The solution structure of the Zα domain of the human RNA editing enzyme ADAR1 reveals a prepositioned binding surface for Z-DNA. *Proc Natl Acad Sci USA* 96:12465–12470.
12. Kahmann JD, et al. (2004) The solution structure of the N-terminal domain of E3L shows a tyrosine conformation that may explain its reduced affinity to Z-DNA in vitro. *Proc Natl Acad Sci USA* 101:2712–2717.
13. Athanasiadis A, et al. (2005) The crystal structure of the Zb domain of the RNA-editing enzyme ADAR1 reveals distinct conserved surface among Z-domains. *J Mol Biol* 351:496–507.
14. Schade M, Turner CJ, Lowenhaupt K, Rich A, Herbert A (1999) Structure-function analysis of the Z-DNA-binding domain Zalpha of dsRNA adenosine deaminase type I reveals similarity to the (α + β) family of helix-turn-helix proteins.. *EMBO J* 18:470–479.
15. Ha SC, et al. (2008) The crystal structure of the second Z-DNA binding domain of human DAI (ZBP1) in complex with Z-DNA reveals an unusual binding mode to Z-DNA. *Proc Natl Acad Sci USA* 105:20671–20676.
16. Ha SC, Lowenhaupt K, Rich A, Kim YG, Kim KK (2005) Crystal structure of a junction between B-DNA and Z-DNA reveals two extruded bases. *Nature* 437:1183–1186.
17. Brandl M, Weiss MS, Jabs A, Sühnel J, Hilgenfeld R (2001) CH-π interactions in proteins. *J Mol Biol* 30:357–377.
18. Ha SC, et al. (2006) Biochemical characterization and preliminary X-ray crystallographic study of the domains of human ZBP1 bound to left-handed Z-DNA. *Biochim Biophys Acta* 1764:320–323.
19. Quyen DV, et al. (2007) Characterization of DNA-binding activity of Z alpha domains from poxviruses and the importance of the beta-wing regions in converting B-DNA to Z-DNA. *Nucleic Acids Res* 35:7714–7720.
20. Kang YM, et al. (2009) NMR spectroscopic elucidation of the B-Z transition of a DNA double helix induced by the Z alpha domain of human ADAR1. *J Am Chem Soc* 131:11485–11491.
21. Ruckert M, Otting G (2000) Alignment of biological macromolecules in novel nonionic liquid crystalline media for NMR experiments. *J Am Chem Soc* 122:7793–7797.
22. Bax A, Kontaxis G, Tjandra N (2001) Dipolar couplings in macromolecular structure determination. *Method Enzymol* 339:127–174.
23. Nietlispach D (2005) Suppression of anti-TROSY lines in a sensitivity enhanced gradient selection TROSY scheme. *J Biomol NMR* 31:161–166.
24. Permi P, Rosevear PR, Annila A (2000) A set of HNCO-based experiments for measurement of residual dipolar couplings in ^{15}N, ^{13}C, (^{2}H) labeled proteins. *J Biomol NMR* 17:43–54.
25. Delaglio F, et al. (1995) NMRPipe: A multidimensional spectral processing system based on UNIX pipes. *J Biomol NMR* 6:277–293.
26. Goddard TD, Kneller DG (2002) SPARKY 3. (University of California, San Francisco).
27. Marat Kirk SpinWorks. (University of Manitoba, Winnipeg, Manitoba, Canada) Version 3.1.7.
28. Güntert P, Mumenthaler C, Wüthrich K (1997) Torsion angle dynamics for NMR structure calculation with the new program DYANA. *J Mol Biol* 273:283–298.
29. Cornilescu G, Delaglio F, Bax A (1999) Protein backbone angle restraints from searching a database for chemical shift and sequence homology. *J Biomol NMR* 13:289–302.
30. Case DA, et al. (2005) The Amber biomolecular simulation programs. *J Comput Chem* 26:1668–1688.
31. Laskowski RA, MacArthur MW, Moss DS, Thornton JM (1993) PROCHECK: A program to check the stereochemical quality of protein structures. *J Appl Crystallogr* 26:283–291.